



Kinetics of skin resealing after insertion of microneedles in human subjects

Jyoti Gupta^a, Harvinder S. Gill^{b,c}, Samantha N. Andrews^b, Mark R. Prausnitz^{a,b,*}

^a School of Chemical & Biomolecular Engineering, Georgia Institute of Technology, Atlanta, Georgia 30332, USA

^b Wallace H. Coulter Department of Biomedical Engineering, Georgia Institute of Technology, Atlanta, Georgia 30332, USA

^c Department of Chemical Engineering, Texas Tech University, Lubbock, Texas 79409, USA

ARTICLE INFO

Article history:

Received 22 January 2011

Accepted 17 May 2011

Available online 26 May 2011

Keywords:

Barrier resealing kinetics

Electrical impedance

Microneedles

Skin permeability

Transdermal drug delivery

ABSTRACT

Over the past decade, microneedles have been shown to dramatically increase skin permeability to a broad range of compounds by creating reversible microchannels in the skin. However, in order to achieve sustained transdermal drug delivery, the extent and duration of skin's increased permeability needs to be determined. In this study, we used electrical impedance spectroscopy to perform the first experiments in human subjects to analyze the resealing of skin's barrier properties after insertion of microneedles. Microneedles having a range of geometries were studied in conjunction with the effect of occlusion to test the hypothesis that increasing microneedle length, number, and cross-sectional area together with occlusion leads to an increase in skin resealing time that can exceed one day. Results indicated that in the absence of occlusion, all microneedle treated sites recovered barrier properties within 2 h, while occluded sites resealed more slowly, with resealing windows ranging from 3 to 40 h depending on microneedle geometry. Upon subsequent removal of occlusion, the skin barrier resealed rapidly. Longer microneedles, increased number of needles, and larger cross-sectional area demonstrated slower resealing kinetics indicating that microneedle geometry played a significant role in the barrier resealing process. Overall, this study showed that pre-treatment of skin with microneedles before applying an occlusive transdermal patch can increase skin permeability for more than one day, but nonetheless allow skin to reseat rapidly after patch removal.

© 2011 Elsevier B.V. All rights reserved.

1. Introduction

Transdermal drug delivery is an attractive alternative to traditional oral and hypodermic delivery, as it overcomes the limitations of first-pass metabolism encountered by oral administration and is safe, painless, and easy to use, in contrast to hypodermic needles [1]. Additionally, the large, accessible surface area of the skin makes it an appealing drug delivery route. Over the past few decades, transdermal patches have been developed to painlessly deliver drugs across the skin. However, the barrier properties offered by the skin's outermost 10–20 μm layer, viz. the stratum corneum, are responsible for poor skin permeability, allowing only a handful of drugs to transport across the skin at therapeutic rates.

Microneedles, which are micron-dimension needles, have been developed to increase skin permeability by creating microchannels in the skin that allow for increased transdermal transport of small and large drug molecules [2,3]. These microneedles are long enough to breach the skin's barrier to allow for drug transport, yet are short enough to avoid stimulating nerves, thereby avoiding pain [4,5].

Over the past decade, several studies have been conducted to show that microneedles are useful for transdermal drug delivery. Microneedles have been used to deliver drugs such as desmopressin [6], plasmid DNA [7], insulin [8], human growth hormone [9] and oligonucleotides [10], as well as vaccines against influenza [11], hepatitis B [7] and C [12], diphtheria [13], anthrax [14] and human papillomavirus [15] in animals [16]. More recently, microneedles have also advanced to human subjects to deliver influenza vaccine [17,18], naltrexone [19], methyl nicotinate [20], topical anesthetics [21] and insulin [22].

Microneedles can be fabricated as single- or multi-needle arrays having hollow channels or solid structures that can be coated with drug or made to encapsulate drug. Hollow microneedles actively deliver drug to the dermis through convective flow, similar to the mechanism of a hypodermic needle. Solid microneedles also deliver drug actively by either inserting drug-encapsulated needles or drug-coated needles into the skin. In each of these active delivery cases, from a safety standpoint it is desirable for the microchannels to close soon after needle removal to prevent permeation of undesired toxic substances or pathogenic microbes that may lead to infection at the treatment site.

Solid microneedles can also deliver drugs via passive diffusion by creating microchannels to increase skin permeability followed by the application of a drug-loaded patch on top of the channels [10,13,19,21,23]. To achieve sustained delivery, from an efficacy

* Corresponding author at: School of Chemical & Biomolecular Engineering, Georgia Institute of Technology, 315 Ferst Drive, Atlanta, GA 30332-0100, USA. Tel.: +1 404 894 5135; fax: +1 404 894 2291.

E-mail address: prausnitz@gatech.edu (M.R. Prausnitz).

standpoint, it is desirable for these microchannels to stay open as long as the drug patch is on the skin. However, it is also desirable for the holes to close quickly after patch removal to prevent site infection.

To achieve prolonged drug delivery using solid microneedles, it is important to determine the extent and duration of the skin's increased permeability because as with any skin wounds or abrasions, the holes created in the skin reseal over time due to the skin's natural repair mechanisms. Upon disruption of the stratum corneum barrier, lamellar body secretion is immediately initiated followed by synthesis of lipids, which are necessary to restore and maintain the stratum corneum barrier [24,25]. Because the kinetics of stratum corneum repair depend on the degree of barrier perturbation [26], it is also important to study stratum corneum repair following treatment with microneedles of various geometries. Further, because the presence of a drug-loaded patch on the treatment site covers (occludes) the skin, it is also necessary to study the effect of occlusion on skin resealing after microneedle treatment.

Previous in-vivo studies performed in hairless guinea pigs have shown that microneedles increased skin permeability over a 48 h time period as characterized by transepidermal water loss [27]. Other studies have also been carried out in human subjects using transepidermal water loss to show that microneedle insertion leads to an increase in skin permeability, but the kinetics of repair were not examined [5,28]. Thus, no kinetic studies have been performed to determine the "window" of increased permeability following microneedle treatment and how it can be modulated.

In this study, we perform the first human experiments to analyze the resealing of skin's barrier properties after microneedle insertion and determine the duration of increased skin permeability as a function of microneedle geometry and skin occlusion. We also study the role of occlusion to influence the expected safety and efficacy of microneedle treatment as well as the relationship between pain and skin resealing time.

Several non-invasive biophysical tools such as transepidermal water loss (TEWL), infrared spectroscopy and electrical impedance spectroscopy have been evaluated to determine the in-vivo integrity of the stratum corneum barrier and permeability of skin [29,30]. Recent studies have also used confocal microscopy and optical coherence tomography to image holes made in the skin using microneedles [31–33]. While TEWL is the most commonly used evaluation tool, this method requires areas studied under occlusion to be un-occluded during the measurement procedure. Because this study specifically tested the effects of occlusion, we employed electrical impedance spectroscopy as our measurement tool so as to allow the occluded treatment sites to remain occluded throughout the experimental period.

The skin's electrical resistance lies predominantly in the stratum corneum and any break in the integrity of the barrier leads to a decrease in skin impedance [34,35], thereby making impedance spectroscopy a useful tool to determine skin barrier integrity after microneedle insertion. Previous studies have demonstrated that there is a strong correlation between skin impedance and skin permeability with a decrease in skin impedance generally corresponding to an increase in skin permeability [36]. Additionally, impedance spectroscopy is a non-invasive and safe measurement tool that is often used in dermatology for the assessment of skin diseases and in the cosmetic industry to study the effect of cosmetics on skin [37].

2. Materials and methods

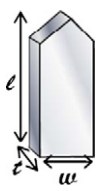
2.1. Microneedle fabrication

Five different microneedle geometries with varying microneedle length, number of needles, and base cross-sectional area (Table 1) were fabricated by laser cutting stainless steel sheets (Trinity Brand Industries, SS 304, 75 μm and 125 μm thick; McMaster-Carr, Atlanta, GA) using previously published methods [38]. The arrays were cleaned and electropolished as described previously [38] and then

Table 1

Parameters of the five different microneedle geometries and two experimental controls studied.

Treatment ¹	Length (<i>l</i>) μm	Thickness (<i>t</i>) μm	Width (<i>w</i>) μm	Number of Microneedles
A	750	75	200	50
B	750	75	200	10
C	500	75	200	50
D	1500	75	200	10
E	750	125	500	50
F	Hypodermic Needle (26 Gauge)			
G	No Treatment			



¹ All treatment conditions, with the exception of treatment F, were studied under occlusive and non-occlusive conditions. Treatment F was only studied in the absence of occlusion.

sterilized in a steam autoclave (Steris Amsco Renaissance 3033 Prevac Steam Sterilizer; Steris Corporation, Mentor, OH). The microneedle arrays had an overall footprint size of 12 mm by 12 mm.

2.2. Electrodes and impedance measurement

Ag/AgCl dry electrodes (Thought Technology T-3404; 25 mm \times 25 mm total area; 10 mm active electrode diameter; Stens Corporation, San Rafael, CA) were used as the measurement electrodes for the treatment sites. A large electrode with a highly conductive gel (Superior Silver Electrode with PermaGel, 70 mm total and active electrode diameter; Tyco Healthcare Uni-Patch, Wabasha, MN) was used as the reference electrode to keep the impedance contribution of the reference site at a negligibly low value. Impedance measurements were made by connecting the reference and measurement electrodes to an impedance meter (EIM-105 Prep-Check Electrode Impedance Meter; General Devices, Ridgefield, NJ) that applied a low frequency (30 Hz) alternating current and was modified with a 200 k Ω resistor (Ack Electronics, Atlanta, GA) in parallel to allow for measurement of skin impedance values greater than 200 k Ω .

2.3. Human subjects

Ten healthy adult human subjects (3 female, 7 male, age: 24–52) with no history of dermatological disease were recruited to participate in this study. Both the left and right volar forearms of all subjects were used in the study. Subjects were asked to refrain from application of any topical formulations or soaps on their arms, as well as to avoid any vigorous physical activity or extreme temperature showers one day prior to and throughout the duration of the experiment. In order to obtain hourly skin impedance data over a period of 48 h after treatment, subjects were divided into two groups of five individuals each. The first group provided data for time points 1–11 and 23–35 h post treatment and the second group generated data for time-points 12–22 and 36–48 h post treatment. Both groups also provided data for time-points –1, –0.5, and 0 (immediately after treatment) h.

Subjects remained in the study room throughout each data collection period. Prior to commencing skin impedance data collection on each study day, subjects were asked to rest in the controlled environment study room for 1 h in order to acclimate to the experimental conditions of 40% relative humidity and room temperature of 21 $^{\circ}\text{C}$. The study was approved by the Georgia Tech Institutional Review Board and all subjects provided informed consent prior to participation.

2.4. Experimental design

A total of 11 sites (left arm: 6 and right arm: 5) were identified on the volar forearms of all ten subjects and were outlined with a pen.

The six sites on the left arm received treatment with microneedles having geometries A, B, and C (see Table 1), three of which were occluded and the remaining three were non-occluded. Of the five sites on the right arm, four received occlusive and non-occlusive treatments with microneedle geometries D and E. At all sites, the microneedles were inserted into the skin manually by pressing the array into the skin for approximately 15–20 s using the thumb of a study investigator. The same investigator applied all microneedles in a similar manner with a consistent force. The application took place such that the microneedles were inserted perpendicular to the surface of the skin. A group of 350 μm -long microneedles were initially included in the study, but they failed to insert into the skin under the conditions used, as shown by insignificant drops in skin impedance. For this reason, those sites (i.e., one site per subject) were treated as no-treatment, negative control sites (G).

The last site on the right arm received non-occlusive treatment using a 26-gage hypodermic needle (treatment F) inserted 5 mm deep into the skin (Becton Dickinson, Franklin Lakes, NJ) and served as the positive control. This site was studied only in the absence of occlusion, because hypodermic needle treated sites are typically left unoccluded in clinical practice. To control the insertion depth, the protective needle cap covering the hypodermic needle was cut such that only 5 mm of the hypodermic needle was protruding from the cap.

The location and order of treatments on the marked skin sites were not randomized and remained consistent among all subjects. The investigators were not blinded to the treatments. The subjects were allowed to watch the procedures and thus knew when a hypodermic needle was inserted as opposed to a microneedle array, but probably could not tell when different microneedle treatments were done, because the various microneedle devices look similar. The treatment sites were arranged such that the reference electrode was at the center of the volar forearm surrounded by the sites with approximately 5 mm edge-to-edge spacing between the reference and the treatment electrodes.

2.5. Experimental procedure

Prior to commencing the study, all subjects were allowed to acclimate to the study environment conditions for a period of 1 h, after which the treatment sites were gently wiped with 70% isopropyl alcohol swabs. The experimental measurement procedure then commenced with a baseline pre-treatment skin impedance recording of the $t = -1$ h reading for all sites by placing the reference and treatment electrodes on their respective sites. Each reading required approximately 30 s to obtain. After data collection, the reference and non-occluded site electrodes were removed. The occluded sites remained covered with the measurement electrode (25 mm \times 25 mm); an occlusive tape (3M Blenderm Surgical Tape; 3M Healthcare, St. Paul, MN) was added to further occlude the sites. Pre-treatment skin impedance measurements were repeated 30 min later at $t = -0.5$ h.

At $t = 0$ h, the occlusive coverings were removed and all sites were administered their respective treatments. Subjects were asked to rate the pain they felt during insertion on a Visual Analog Scale ranging from 0 to 10 with 0 being no pain and 10 corresponding to worst pain. Electrodes were immediately placed on the sites and impedance measurements were recorded (the occluded sites were covered again). Measurements were taken on the two subject groups to generate impedance data up to 48 h post treatment. After the 42nd hour reading, all occlusive dressings were removed and all sites remained non-occluded for the last 6 h. At the end of each study day, the occluded sites were further covered with a waterproof dressing (Nexcare Absolute Waterproof Premium Adhesive Pad, 3M Healthcare) and with an occlusive film of polyvinylidene chloride (Saran Wrap; SC Johnson, Racine, WI) which was secured with

waterproof tape (Nexcare Absolute Waterproof First Aid Tape; 3M Healthcare) to ensure complete occlusion when subjects went home for the night.

2.6. Calculation of total permeable area and drug concentration

The permeable area of skin available for drug transport after microneedle treatment was calculated using the following relation:

$$A_{\text{permeable}} = \frac{\rho L}{Z} \quad (1)$$

where $A_{\text{permeable}}$ is the total permeable area of all microchannels created by an array, ρ is the electrical resistivity of interstitial fluid in the skin ($\sim 78 \Omega\text{-cm}$ [39]), L is the length of the diffusional pathways in the stratum corneum ($\sim 15 \mu\text{m}$, which is an estimate of the average thickness of the stratum corneum [1]), and Z is the absolute skin impedance measured during the study.

Using data from a separate study [19], the concentration (c) of naltrexone in the body over time (t) after microneedle treatment was determined from the following single-compartment model:

$$\frac{dc}{dt} = \frac{N\rho D\Delta C_{\text{patch}}}{V_{\text{dist}}Z(t)} - \frac{Cl c(t)}{V_{\text{dist}}} \quad (2)$$

where N is a correction factor corresponding to the area of microneedle arrays in the clinical naltrexone study [19] divided by the area of arrays in this impedance study (i.e. 8/1), D is the diffusion coefficient for naltrexone in water calculated from the Stokes–Einstein equation ($= 4.6 \times 10^{-6} \text{ cm}^2/\text{s}$ using a molecular diameter of 9.15 Å for naltrexone [40]), ΔC_{patch} is the difference in naltrexone concentration in the patch and in the body ($\sim 160 \text{ mg/mL}$ [19]), V_{dist} is the apparent volume of distribution for naltrexone ($\sim 1350 \text{ L}$ [41]), $Z(t)$ is the absolute skin impedance measured in this study, and Cl is the total body clearance of naltrexone ($\sim 3.5 \text{ L/min}$ [41]).

This equation indicates that the rate of change of the plasma naltrexone concentration is equal to the rate of naltrexone absorption (first term on right hand side of equation) minus the rate of elimination (second term on right hand side of equation). The absorption term containing impedance was derived from Fick's first law of diffusion, where flux across skin is given by $J = K_p \Delta C$. K_p is the permeability of skin treated with microneedles and is defined by $K_p = f \times D/L$ [42]. In this equation, f is the fractional skin area containing holes from microneedles and can be expressed as $A_{\text{permeable}}/A$, where $A_{\text{permeable}}$ is given by Eq. (1) and A is the area of the microneedle array. This flux term containing impedance was multiplied by the area of the arrays used in the naltrexone study and divided by the volume of distribution to arrive at the rate of absorption term. The elimination term was simply defined as the elimination rate constant (Cl/V_{dist}) multiplied by the plasma naltrexone concentration, as commonly used in pharmacokinetic analysis [43]. Therefore, all parameters in this model are based on properties of the drug and skin and the model does not contain any fitted parameters.

2.7. Statistical methods

One- and two-way repeated measures ANOVA were performed using NCSS 2007 (NCSS, Kaysville, UT). Analysis of the occluded and non-occluded data over all time points and for all needle geometries was performed using the general linear model (GLM) ANOVA using Minitab 15 (Minitab Inc., State College, PA). Tukey's post hoc pairwise comparisons were performed to compare which factor levels led to significant differences. Comparisons of goodness of fit between experimental observations and predicted results were performed using the χ^2 test with 12 degrees of freedom (12 experimental

measurement points). In all cases, a value of $p < 0.05$ was considered statistically significant.

3. Results and discussion

Microneedles are known to increase skin permeability to a wide range of molecules by creating microchannels in the skin. In this study, we quantify that effect using impedance spectroscopy and determine the lifetime of transdermal transport pathways by testing the hypothesis that increasing microneedle length, number, and base cross-sectional area in conjunction with occlusion leads to an increase in skin resealing time that can exceed one day.

3.1. Effect of microneedle geometry on initial skin impedance drop

The left and right volar forearms of 10 healthy adult human subjects were used in this study. Five different microneedle geometries (Table 1) with varying length, number, thickness, and width (geometries A–E) were studied under occlusive (impermeable to air and moisture) and non-occlusive conditions, and compared to positive (F, hypodermic needle) and negative (G, no treatment) controls. A total of 11 sites (5 occluded, 6 non-occluded) were identified and marked.

Fig. 1 shows a microneedle array used in this study and depicts the treatment sites on the arm. Pre-treatment impedance measurements were taken at the beginning of the study, after which the marked sites on each subject were administered their respective treatments at time $t = 0$ h, followed by hourly skin impedance measurements. The impedance values were then normalized with respect to their corresponding positive control hypodermic needle (F) impedance to account for inter-subject variability.

To determine the effect of microneedle geometry on the initial drop in skin impedance as compared to that caused by a 26-gauge hypodermic needle (F), the average normalized skin impedance Z_{norm} for each of the treatment conditions (A–G) at time $t = 0$ h was analyzed (Fig. 2). The impedance values for the microneedle (A–E) and hypodermic needle (F) sites were all significantly lower than that of the no treatment control (G) (repeated measures one-way ANOVA, $p < 0.05$), however, there were no significant differences among treatments A–F (repeated measures one-way ANOVA, $p > 0.05$). Since intact human skin is generally characterized by high electrical impedance that is attributed primarily to the stratum corneum, these low impedance values are consistent with the expectation that microneedle insertion breached the stratum corneum barrier. Further, although we anticipated that more needles and needles with larger cross-sectional area would make more/bigger holes, which would lead to lower initial impedance at $t = 0$ h, comparisons between geometries A and B, and A and E revealed no significant difference in initial impedances, perhaps due to the relatively large error bars. However, we hypothesize that larger changes in needle width and number of needles would make a significant difference. These changes might also make microneedle insertion more difficult.

3.2. Kinetics of skin barrier resealing: effect of occlusion

To determine the duration of the increased skin permeability caused by microneedles, skin impedance profiles for all microneedle geometries were measured and analyzed in the presence and absence of occlusion over a 48 h experimental period. The impedance data for each subject were normalized with respect to their corresponding $t = 0$ positive control (F) and the average normalized impedance was plotted over time for both the occluded and non-occluded cases as shown in Fig. 3. From these data, the kinetics of skin resealing can be determined as a function of microneedle geometry and skin occlusion.

Analysis of the effect of occlusion on skin resealing was performed in two ways. First, the impedance profiles for the occluded and non-

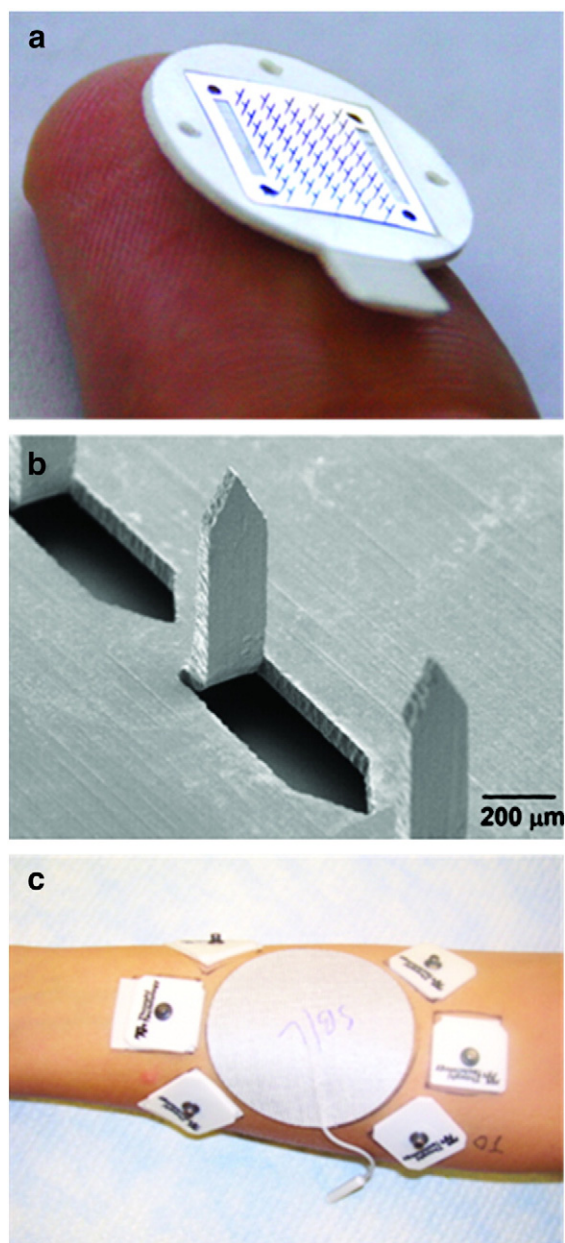


Fig. 1. Representative microneedles used for insertion in human forearms. (a) Brightfield micrograph of a 50 microneedle array (treatment A), (b) scanning electron micrograph of a section of the 50 microneedle array, (c) experimental set-up of the left volar forearm of a human subject: a large, highly conductive, gelled central reference electrode surrounded by dry Ag/AgCl measurement electrodes placed on treatment sites. Impedance measurements were made by periodically connecting reference and measurement electrodes to an impedance meter.

occluded sites were compared up to the 42 h time point (at which point occlusion was removed from all occluded sites). As can be seen from Fig. 3, the impedance values for both the occluded and non-occluded cases dropped significantly from their pre-treatment values immediately after needle insertion and then increased over time indicating skin barrier resealing. However, the speed of this resealing depended on the occlusive condition of the skin and on microneedle geometry. Comparison of the occluded and non-occluded cases over all time-points indicated that skin resealing was significantly faster in the absence of occlusion (GLM ANOVA followed by Tukey's pairwise comparison, $p < 0.05$).

In addition, the data for the occluded sites (Fig. 3a) were analyzed before and after removal of occlusion at the 42nd hour. This

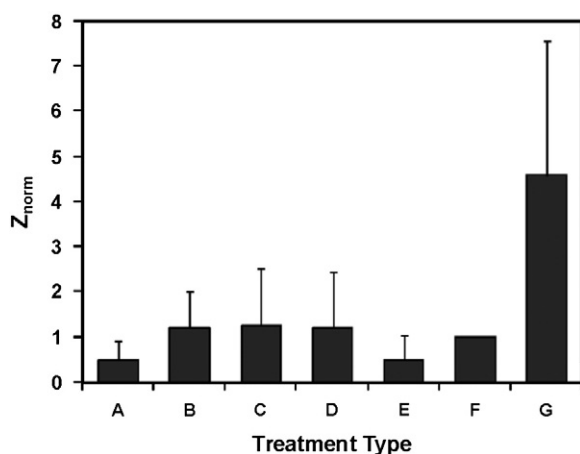


Fig. 2. Comparison of normalized (relative to hypodermic needle positive control, treatment F) average skin impedance (Z_{norm}) values at time = 0 h (immediately after treatment) for the different treatment conditions (see Table 1). A significant reduction in skin resistance upon treatment with microneedles (A–E) and hypodermic needle (F) was observed in comparison to the intact skin negative control (G). There was no significant difference among treatments A–F. Data expressed as mean \pm SD; $n = 20$.

evaluation revealed that upon removal of occlusion after the 42nd hour, the skin impedance immediately increased within 1 h (two-way ANOVA followed by Tukey's pairwise comparison, $p < 0.05$), again showing that skin resealing was significantly faster in the absence of occlusion.

We hypothesize that this slow barrier resealing under occlusion is due to the reduced transepidermal water loss under occlusive skin conditions. Previous studies have shown that stratum corneum barrier repair is regulated by the formation of a water gradient in the skin caused by increased transepidermal water loss through the compromised skin barrier (Grubauer et al. 1989). Occluding the skin with a vapor impermeable membrane introduces an artificial skin barrier and eliminates this gradient. As a result, the secretion of lamellar bodies and lipid synthesis, which are essential to repair and regulate the stratum corneum barrier, are significantly retarded, leading to prolonged barrier recovery [24,25]. Additionally, under occlusion, the skin becomes significantly hydrated. Hydration is the primary variable influencing the skin's impedance, with increased stratum corneum hydration leading to a reduction in skin impedance [29,37]. It should be noted that skin resealing reported in this study, as determined by electrical impedance, is a measure of skin barrier property recovery, which is probably not the same as full healing of skin anatomy and physiology.

This switch-like behavior where microneedle-generated channels remain open under occlusion but close rapidly after removal of occlusion gives insight into the safety and efficacy of drug delivery approaches based on microneedle pretreatment followed by application of a topical patch, as described earlier. This finding suggests that a drug-loaded occlusive patch can be applied to the skin immediately after microneedle treatment to enable prolonged drug delivery, followed by rapid skin resealing and termination of delivery upon patch removal. Additionally, the fast resealing of microneedle holes in the absence of occlusion reduces the chance of infection at the insertion site, which should increase safety of non-occlusive active-delivery microneedle systems such as hollow, drug-coated, and drug-encapsulating microneedles.

Fig. 3a also shows that the no-treatment negative control line (G) gradually decreased during the first 10–12 h and then remained relatively constant for the remainder of the study until occlusion was removed. This reduction in impedance was due to the increased hydration of the skin under occlusion as described above. The non-occluded negative control on the other hand did not show this

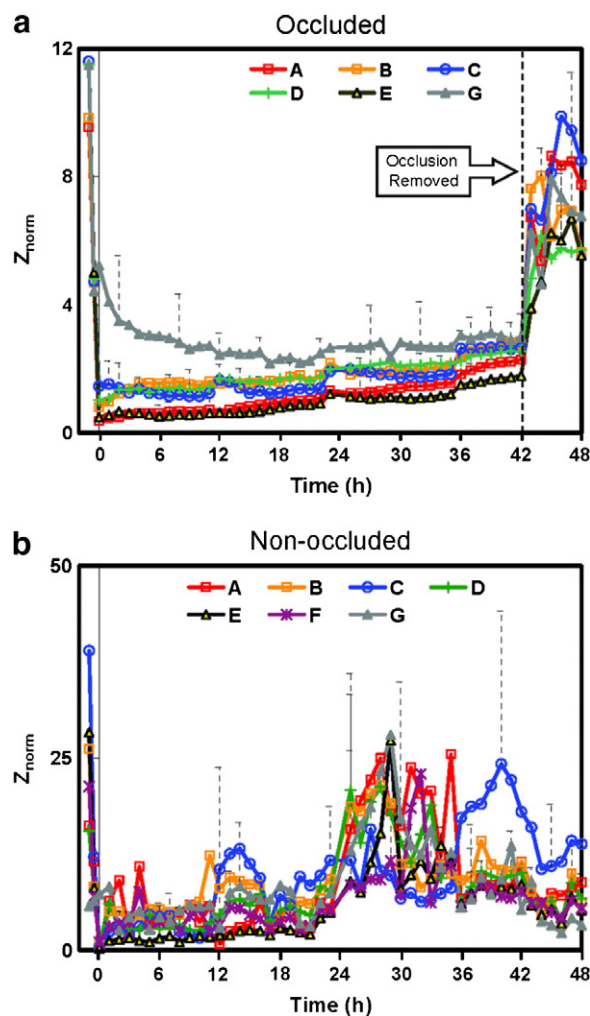


Fig. 3. Normalized (relative to hypodermic needle positive control impedance at $t = 0$, treatment F) average skin impedance (Z_{norm}) profile over the course of a 48 h time period for different skin treatments (see Table 1). Profile (a) under occlusion and (b) without occlusion. Occlusion led to a slower resealing of skin impedance on the order of several hours to more than one day for all treatment conditions when compared to non-occluded sites. Upon removal of occlusion, skin impedance rapidly increased. Graphs expressed as mean \pm SD; $n = 5$ for $t > 0$, $n = 10$ for $t \leq 0$. See Supplemental Information Fig. S1 for additional graphs directly comparing occluded and non-occluded skin impedance data for each treatment.

reduction in impedance, but rather, showed an erratic noisy behavior (Fig. 3b). This was also true for the non-occluded treated sites once they resealed (A–F). While the underlying reason for the erratic behavior is not known, this could be due to a measurement artifact caused by inconsistent electrical contact between the dry skin and dry electrodes. For intact skin with high impedance, even a small change in the barrier or its hydration can have a large effect on the impedance value. In contrast, compromised skin with low impedance is relatively insensitive to such small changes. Mathematically, this effect comes from the reciprocal relationship between skin permeability (P) and electrical impedance (Z) (i.e. $P \sim 1/Z$). If the graph is re-plotted with electrical admittance (Y) on the y-axis (i.e. $Y = 1/Z$), then the noise in Fig. 3b is dramatically reduced (data not shown).

3.3. Kinetics of skin barrier resealing: effect of microneedle geometry

This study also hypothesized that increasing microneedle length, number, thickness, and width leads to an increase in skin barrier resealing time. In order to test this hypothesis and to determine the time for the channels created by microneedles to reseat, the

impedance profiles for each treatment type were compared with that of the no-treatment negative control (G). The skin resealing time (Table 2) was determined as the time at which there was no significant difference between the treatment and negative control sites. This comparison controlled for the effects of hydration due to occlusion (in the case of the occluded sites) and thereby identified effects of the treatment itself.

Analysis of the occluded data revealed that the window of increased permeability showed strong dependence on microneedle geometry (Table 2). The non-occluded data on the other hand revealed that for all needle treatment conditions (A–F), the skin impedance increased rapidly and within 2 h of treatment, skin was resealed with no dependence on needle geometry.

To further elucidate the effect of microneedle geometry parameters on skin resealing under occlusion, we compared the resealing times based on changes in length, number, and cross-sectional area of microneedles as seen in Table 2 and Fig. 4. Doubling the microneedle length while keeping other parameters constant led to a 6-fold increase in skin resealing time as revealed by comparison of geometries B (750 μm length) and D (1500 μm length). Further, comparing geometries C (500 μm length) and A (750 μm length) indicated that a 50% increase in microneedle length, while holding other parameters constant, led to approximately 35% increase in skin resealing time. Both these comparisons are consistent with the hypothesis that increasing microneedle length increases skin barrier resealing time under the effect of occlusion.

The number of microneedles also affected skin resealing time with a 5-fold increase in number of needles corresponding to a 10-fold increase in barrier resealing time demonstrated by comparing geometries B (10-needle array) and A (50-needle array) (Fig. 4). Further, a 4-fold increase in cross-sectional area led to a 33% increase in resealing time as shown by comparing geometries A ($w = 200 \mu\text{m}$, $t = 75 \mu\text{m}$) and E ($w = 500 \mu\text{m}$, $t = 125 \mu\text{m}$). Under occlusion, microneedles with geometry E had the longest skin resealing time of 40 h. These results validated that increasing microneedle number and cross-sectional area led to an increase in barrier resealing time under occlusion.

In the small array (10 needles), increasing needle length (treatment B vs. D) and increasing number of needles (treatment B vs. A) both dramatically increased resealing time. In the large array (50 needles), increasing needle length (treatment C vs. A) and increasing needle cross-sectional area (treatment A vs. E) both had much smaller effects on resealing time. This suggests that very minor injury from a small number of short needles (treatment B) can be quickly repaired, but injury beyond some threshold exceeded by increasing needle length and/or number of needles significantly slows the repair process from a few hours to on the order of one day. Alternatively, the method of statistical analysis may have influenced these reported differences. Closer examination of the microneedle

Table 2
Skin resealing time and pain as a function of needle geometry and skin occlusion.

Treatment	Time (h) ¹		Pain ²
	Occluded	Non-occluded	
A	30	2	0.52 ± 0.14
B	3	2	0.31 ± 0.17
C	22	2	0.33 ± 0.13
D	18	2	0.85 ± 0.10
E	40	2	0.53 ± 0.14
F	n/a	2	1.0

¹ Time to achieve non-significant difference of skin impedance from negative control. These data were obtained by determining the times at which the average impedance of needle-treated skin was statistically indistinguishable from the average no-treatment negative control (treatment G) using the data in Fig. 3.

² Visual Analog Scale (VAS) pain score normalized to the hypodermic needle (F) positive control; VAS scores expressed as mean ± SD of occluded and non-occluded treatments, i.e. $n = 20$ for A–E and $n = 10$ for F.

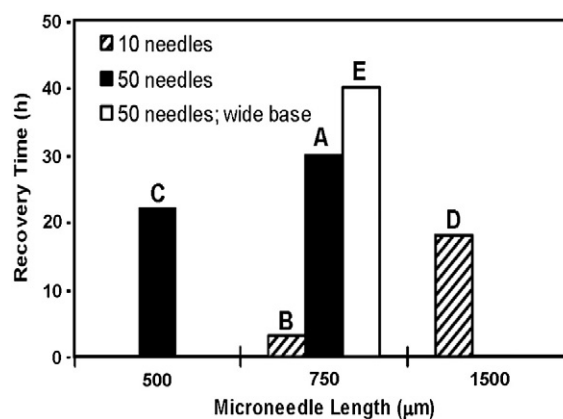


Fig. 4. Comparison of skin barrier resealing time under occlusion based on microneedle length, number of microneedles, and cross-sectional area. Treatment E with 50 microneedles having length 750 μm , width 500 μm , and thickness 125 μm had the slowest resealing at 40 h under occlusion. These data were obtained by determining the times at which the average impedance of microneedle-treated skin was statistically indistinguishable from the average no-treatment negative control (treatment G) using the data in Fig. 3.

curves in Fig. 3 shows that they all have similar slopes, suggesting similar resealing rates. The differences in resealing times reported in Table 2 may be influenced by the different initial impedance drops and the relatively large error bars, and thus the actual differences in resealing times may not be as dramatic as reported in Table 2.

3.4. Relationship between microneedle geometry, resealing time, and pain

Overall, under occlusion, skin resealing depended on microneedle length, number, and cross-sectional area with length and number having the most sensitive effects. While these parameters have strong effects in increasing skin resealing time, they also have a significant effect on pain. We therefore hypothesized that microneedles causing increased resealing time also cause increased pain, because both are secondary measures of tissue injury.

To test this hypothesis, we asked the subjects to report the Visual Analog Scale (VAS) pain scores felt during each microneedle insertion. The pain scores for each subject were then normalized with respect to their corresponding hypodermic needle positive control (F) (Table 2). Overall, all microneedle geometries with the exception of D were significantly less painful than the hypodermic needle control, F (one-way ANOVA followed by Tukey's pairwise comparison, $p < 0.05$), and all microneedle geometries with the exception of D were not significantly different from each other (one-way ANOVA followed by Tukey's pairwise comparison, $p > 0.05$). This finding is consistent with previous measurements of pain caused by microneedles, which showed that microneedle length is the most important factor [4].

This finding also indicates that although varying microneedle length, number and area all affected skin resealing time, only microneedle length affected pain, over the range of parameters considered. These observations are inconsistent with our proposed hypothesis and suggest that aspects of tissue injury caused by microneedles that affect pain are different from those which affect resealing time. This could be explained because pain is influenced by a direct interaction between microneedles and sensory nerve fibers, whereas resealing time is influenced by damage to the stratum corneum, which is devoid of nerves. The finding that skin resealing time and pain are not directly coupled presents opportunities to design microneedle devices that cause prolonged skin permeability (under occlusion), but still cause little or no pain. It appears that using larger numbers of needles with larger cross-sectional area, rather than long needles, can accomplish this goal (e.g., treatment E).

3.5. Estimation of permeable microchannel area over time

We next sought to estimate the permeable area of skin available for drug transport after microneedle treatment. To do this, we assumed that the channels created by microneedles have a non-tapered geometry and then correlated the total pore size to skin impedance using Eq. (1) described in the Materials and Methods section. We determined the total permeable area for the various microneedle patch geometries at $t=0$ h to range from $1.9 (\pm 0.4) \times 10^{-4} \text{ mm}^2$ to $6.6 (\pm 0.8) \times 10^{-4} \text{ mm}^2$, which is smaller than the cross-section of an adult human hair ($7.9 \times 10^{-3} \text{ mm}^2$ [44]).

The area of the hole made by each individual microneedle in a 10- or 50-needle array is expected to be 1/10 or 1/50 of the predicted total area on average. These areas correspond to effective microchannel radii of approximately $2 \mu\text{m}$ (assuming a circular cross section), which is in general agreement with a previous estimate of effective microchannel size made by a different method [42]. This microchannel size is 1–2 orders of magnitude smaller than the cross-sectional dimensions of the microneedles used in this study, which suggests significant shrinking of microchannels after microneedle removal due to skin's elasticity, which is consistent with previous observations [32,42].

Over time, as skin impedance increased, the total permeable area decreased until it was indistinguishable from the negative control. The area associated with the negative control, which is a measure of normal skin imperfections and experimental noise, was found to be $4.6 (\pm 2.1) \times 10^{-5} \text{ mm}^2$, which was considered to be resealed.

To validate these predictions of microchannel area, we compared our data to an independent study carried out to deliver naltrexone to human subjects after treatment with the same microneedles used in this study [19]. In that study, two microneedle arrays with geometry A were inserted four times each into the forearm of six healthy subjects to create a total of 400 microchannels per subject. A naltrexone gel patch was then placed over the treated area and covered by an occlusive dressing for 72 h. Data from that study show that plasma naltrexone concentration increased over the first few hours and then held relatively steady for the remaining 72 h study.

As a first comparison, our study found that the resealing time for microneedle geometry A was 30 h, which contrasts with the finding by Wermeling et al. that naltrexone concentration remained elevated for at least 72 h. This result, however, can be explained by the fact that Wermeling et al. inserted arrays of microneedle geometry A a total of 8 times into the skin (i.e., 400 microchannels), whereas our prediction of skin resealing is based on a single insertion (i.e., 50 microchannels). Given the strong dependence of skin resealing on the number of microneedles seen when comparing a 10-needle array to a 50-needle array (Fig. 4), increasing from 50 needles to, effectively, 400 needles could further increase resealing time. In addition, our impedance data measured the time taken for the stratum corneum barrier to repair, whereas Wermeling et al. measured the kinetics of plasma naltrexone levels. Plasma drug levels are influenced not only by stratum corneum permeability, but also by drug diffusion through the skin and into the bloodstream and by drug elimination from the bloodstream, which has a half-life of 4.4 h [19], and from a possible drug depot within the skin often associated with transdermal delivery.

To provide a more detailed comparison between the naltrexone data and our predictions of drug delivery based on skin impedance measurements, we developed a single-compartment pharmacokinetic model (Eq. (2)) to predict plasma naltrexone concentration over time. Fig. 5 shows plasma naltrexone concentration profiles over a 30 h period from the experimental study [19] and from Eq. (2). As seen in the figure, both graphs show an initial increase in naltrexone concentrations and then remained relatively steady. The peak concentration from the naltrexone delivery experiment by Wermeling et al. was found to be $4.5 \pm 2.5 \text{ ng/mL}$ and the time to this peak was $8.8 \pm 7.6 \text{ h}$. The predicted naltrexone profile led to a peak

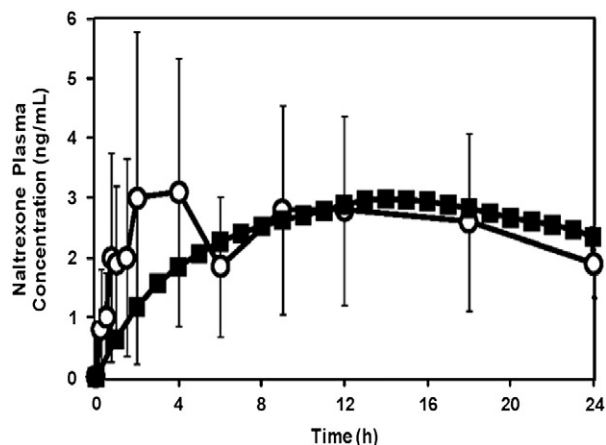


Fig. 5. Plasma concentrations of naltrexone from (○) an experimental study involving delivery of naltrexone to human subjects, and from (■) theoretical prediction using Eq. (2). The predicted data are in agreement with the experimental results. Experimental data are expressed as mean \pm SD taken direction from Ref. [19].

concentration of 3 ng/mL at 13 h, which lies within the range of experimental error for the clinical delivery study. Further, a χ^2 test to compare the experimental plasma concentrations of naltrexone by Wermeling et al. and the predicted concentrations from Eq. (2) revealed that the predicted data is in agreement with the experimental observations ($\chi^2 = 5.16 < \chi^2_{\text{critical value}} = 21.06$). These results indicate that skin impedance can be used to predict drug concentrations in the body after microneedle-based delivery to within the accuracy of the experimental data.

4. Conclusions

This study supported the hypothesis that increasing microneedle length, number, and cross-sectional area in conjunction with occlusion leads to an increase in skin resealing time that can exceed one day. Results indicated that occlusion significantly retards skin barrier resealing after microneedle treatment. However, skin rapidly reseals in the absence of occlusion. The study also revealed that the initial degree of skin permeabilization created by microneedles is relatively insensitive to the length, number, or cross-sectional area of the microneedles. However, these parameters do play a significant role in the stratum corneum resealing process. Longer, increased number, and larger cross-sectional area needles resealed more slowly under the effect of occlusion. Analysis of pain scores demonstrated that only increasing microneedle length increased pain, which suggests that the duration of increased skin permeability can be extended without increasing pain by increasing the number of microneedles rather than their length. Overall, this study demonstrated that microneedles can be used to increase skin permeability over timescales ranging from as little as 2 h to as long as 40 h. This study also validated that skin impedance measurements can be used to predict transdermal flux in human subjects. Additional studies with a larger population of human subjects and using additional methods of analysis, such as TEWL and microscopic imaging, should be used to further validate these findings.

The findings of this study have implications for both passive and active microneedle delivery systems. From an efficacy standpoint, piercing skin with microneedles can provide increased skin permeability to facilitate drug delivery from a transdermal patch over a period of almost 2 days. However, increased skin permeability can be quickly reversed in the absence of occlusion due to the rapid skin resealing that occurs under these conditions. This simple dependence of skin permeability on skin occlusion provides an inherent safety feature that allows skin to reseat rapidly after removal of

microneedles at the end of an active delivery process (e.g. injection) or after patch removal following passive drug delivery through long-lived microchannels.

Acknowledgements

We acknowledge Richard Shafer for training and assistance in infrared laser operation, Mark Allen for access to his laser fabrication facilities and Vladimir Zarnitsyn for helpful discussions. We acknowledge Sontra Medical Corporation (now Echo Therapeutics) and the National Institutes of Health for financial support. This work was carried out at the Center for Drug Design, Development and Delivery and the Institute for Bioengineering and Bioscience at the Georgia Institute of Technology. MRP serves as a consultant and MRP and HSG are inventors on patents licensed to companies developing micro-needle-based products. This potential conflict of interest has been disclosed and is being managed by Georgia Tech and Emory University.

Appendix A. Supplementary data

Supplementary data to this article can be found online at doi:10.1016/j.jconrel.2011.05.021.

References

- [1] M.R. Prausnitz, R. Langer, Transdermal drug delivery, *Nat. Biotechnol.* 26 (11) (2008) 1261–1268.
- [2] M.R. Prausnitz, H.S. Gill, J.-H. Park, in: M.J. Rathbone, J. Hadgraft, M.S. Roberts, M.E. Lane (Eds.), *Modified Release Drug Delivery*, Vol. 2, Informa Healthcare, New York, 2008, pp. 295–309.
- [3] R.F. Donnelly, T.R. Raj Singh, A.D. Woolfson, Microneedle-based drug delivery systems: microfabrication, drug delivery, and safety, *Drug Deliv.* 17 (4) (2010) 187–207.
- [4] H.S. Gill, D.D. Denson, B.A. Burris, M.R. Prausnitz, Effect of microneedle design on pain in human volunteers, *Clin. J. Pain* 24 (7) (2008) 585–594.
- [5] M.I. Haq, E. Smith, D.N. John, M. Kalavala, C. Edwards, A. Anstey, A. Morrissey, J.C. Birchall, Clinical administration of microneedles: skin puncture, pain and sensation, *Biomed. Microdevices* 11 (1) (2009) 35–47.
- [6] M. Cormier, B. Johnson, M. Ameri, K. Nyam, L. Libiran, D.D. Zhang, P. Daddona, Transdermal delivery of desmopressin using a coated microneedle array patch system, *J. Control. Release* 97 (3) (2004) 503–511.
- [7] F. Chabri, K. Bouris, T. Jones, D. Barrow, A. Hann, C. Allender, K. Brain, J. Birchall, Microfabricated silicon microneedles for nonviral cutaneous gene delivery, *Br. J. Dermatol.* 150 (5) (2004) 869–877.
- [8] K. Fukushima, T. Yamazaki, R. Hasegawa, Y. Ito, N. Sugioka, K. Takada, Pharmacokinetic and pharmacodynamic evaluation of insulin dissolving microneedles in dogs, *Diabetes Technol. Ther.* 12 (6) (2010) 465–474.
- [9] J.W. Lee, S.O. Choi, E.I. Felner, M.R. Prausnitz, Dissolving microneedle patch for transdermal delivery of human growth hormone, *Small* 7 (4) (2011) 531–539.
- [10] W. Lin, M. Cormier, A. Samiee, A. Griffin, B. Johnson, C. Teng, G.E. Hardee, P. Daddona, Transdermal delivery of antisense oligonucleotides with microprojection patch (Macroflux) technology, *Pharm. Res.* 18 (12) (2001) 1789–1793.
- [11] S.P. Sullivan, D.G. Koutsonanos, M. Del Pilar Martin, J.W. Lee, V. Zarnitsyn, S.O. Choi, N. Murthy, R.W. Compans, I. Skountzou, M.R. Prausnitz, Dissolving polymer microneedle patches for influenza vaccination, *Nat. Med.* 16 (8) (2010) 915–920.
- [12] H.S. Gill, J. Soderholm, M.R. Prausnitz, M. Sallberg, Cutaneous vaccination using 690 microneedles coated with hepatitis C DNA vaccine, *Gene Ther.* 17 (6) (2010) 811–814.
- [13] Z. Ding, F.J. Verbaan, M. Bivas-Benita, L. Bungener, A. Huckriede, D.J. van den Berg, G. Kersten, J.A. Bouwstra, Microneedle arrays for the transcutaneous immunization of diphtheria and influenza in BALB/c mice, *J. Control. Release* 136 (1) (2009) 71–78.
- [14] J.A. Mikszta, V.J. Sullivan, C. Dean, A.M. Waterston, J.B. Alarcon, J.P. Dekker III, J.M. Brittingham, J. Huang, C.R. Hwang, M. Ferriter, G. Jiang, K. Mar, K.U. Saikh, B.G. Stiles, C.J. Roy, R.G. Ulrich, N.G. Harvey, Protective immunization against inhalational anthrax: a comparison of minimally invasive delivery platforms, *J. Infect. Dis.* 191 (2) (2005) 278–288.
- [15] H.J. Corbett, G.J. Fernando, X. Chen, I.H. Frazer, M.A. Kendall, Skin vaccination against cervical cancer associated human papillomavirus with a novel micro-projection array in a mouse model, *PLoS One* 5 (10) (2010) e13460.
- [16] M.R. Prausnitz, J.A. Mikszta, M. Cormier, A.K. Andrianov, in: R.W. Compans, W.A. Orenstein (Eds.), *Vaccines for pandemic influenza*, Springer, Berlin, 2009, pp. 369–393.
- [17] P. Van Damme, F. Oosterhuis-Kafeja, M. Van der Wielen, Y. Almagor, O. Sharon, Y. Levin, Safety and efficacy of a novel microneedle device for dose sparing intradermal influenza vaccination in healthy adults, *Vaccine* 27 (3) (2009) 454–459.
- [18] D. Holland, R. Booy, F. De Looze, P. Eizenberg, J. McDonald, J. Karrasch, M. McKeirnan, H. Salem, G. Mills, J. Reid, F. Weber, M. Saville, Intradermal influenza vaccine administered using a new microinjection system produces superior immunogenicity in elderly adults: a randomized controlled trial, *J. Infect. Dis.* 198 (5) (2008) 650–658.
- [19] D.P. Wermeling, S.L. Banks, D.A. Hudson, H.S. Gill, J. Gupta, M.R. Prausnitz, A.L. Stinchcomb, Microneedles permit transdermal delivery of a skin-impermeant medication to humans, *Proc. Natl. Acad. Sci. U. S. A.* 105 (6) (2008) 2058–2063.
- [20] R.K. Sivamani, B. Stoerber, G.C. Wu, H. Zhai, D. Liepmann, H. Maibach, Clinical microneedle injection of methyl nicotinate: stratum corneum penetration, *Skin Res. Technol.* 11 (2) (2005) 152–156.
- [21] X. Li, R. Zhao, Z. Qin, J. Zhang, S. Zhai, Y. Qiu, Y. Gao, B. Xu, S.H. Thomas, Microneedle pretreatment improves efficacy of cutaneous topical anesthesia, *Am. J. Emerg. Med.* 28 (2) (2010) 130–134.
- [22] J. Gupta, E.I. Felner, M.R. Prausnitz, Minimally invasive insulin delivery in type 1 diabetic subjects using hollow microneedles, *Diabetes Technol. Ther.* 11 (6) (2009) 329–337.
- [23] S. Henry, D.V. McAllister, M.G. Allen, M.R. Prausnitz, Microfabricated microneedles: a novel approach to transdermal drug delivery, *J. Pharm. Sci.* 87 (8) (1998) 922–925.
- [24] G. Grubauer, P.M. Elias, K.R. Feingold, Transepidermal water loss: the signal for recovery of barrier structure and function, *J. Lipid Res.* 30 (1989) 323–333.
- [25] G.K. Menon, K.R. Feingold, P.M. Elias, Lamellar body secretory response to barrier disruption, *J. Invest. Dermatol.* 98 (3) (1992) 279–289.
- [26] H. Schaefer, T.E. Redelmeier, *Skin barrier: principles of percutaneous absorption*, Karger, Basel, 1996.
- [27] S.L. Banks, R.R. Pinninti, H.S. Gill, K.S. Paudel, P.A. Crooks, N.K. Brogden, M.R. Prausnitz, A.L. Stinchcomb, Transdermal delivery of naltrexol and skin permeability lifetime after microneedle treatment in hairless guinea pigs, *J. Pharm. Sci.* 99 (7) (2010) 3072–3080.
- [28] S.M. Bal, J. Caussin, S. Pavel, J.A. Bouwstra, *In-vivo* assessment of safety of microneedle arrays in human skin, *Eur. J. Pharm. Sci.* 35 (3) (2008) 193–202.
- [29] C. Curdy, A. Naik, Y.N. Kalia, I. Alberti, R.H. Guy, Non-invasive assessment of the effect of formulation excipients on stratum corneum barrier function *in-vivo*, *Int. J. Pharm.* 271 (1–2) (2004) 251–256.
- [30] J. Fluhr, P. Elsner, E. Berardesca, H.I. Maibach, *Bioengineering of the skin: water and the stratum corneum*, CRC Press, Boca Raton, 2005.
- [31] S. Bal, A. Kruthof, H. Liebl, M. Tomerius, J. Bouwstra, J. Lademann, M. Meinke, *In vivo* visualization of microneedle conduits in human skin using laser scanning microscopy, *Laser Phys. Lett.* 7 (3) (2010) 242–246.
- [32] S. Coulman, J. Birchall, A. Alex, M. Pearton, Hofer, C. O'Mahony, W. Drexler, B. Povazay, *In vivo*, in situ imaging of microneedle insertion into the skin of human volunteers using optical coherence tomography, *Pharm. Res.* 28 (1) (2011) 66–81.
- [33] G. Li, A. Badkar, H. Kalluri, A. Banga, Microchannels created by sugar and metal microneedles: characterization by microscopy, macromolecular flux and other techniques, *J. Pharm. Sci.* 99 (4) (2010) 1931–1941.
- [34] T. Yamamoto, Y. Yamamoto, Electrical properties of the epidermal stratum corneum, *Med. Biol. Eng. (Mar.)* (1976) 151–158.
- [35] M.R. Prausnitz, The effects of electric current applied to the skin: a review for transdermal drug delivery, *Adv. Drug Deliv. Rev.* 18 (1996) 395–425.
- [36] P. Karande, A. Jain, S. Mitragotri, Relationships between skin's electrical impedance and permeability in the presence of chemical enhancers, *J. Control. Release* 110 (2) (2005) 307–313.
- [37] R.R. Burnette, J.D. DeNuzzio, in: R.O. Potts, R.H. Guy (Eds.), *Mechanisms of transdermal drug delivery*, Marcel Dekker, New York, 1997, pp. 215–230.
- [38] H.S. Gill, M.R. Prausnitz, Coated microneedles for transdermal delivery, *J. Control. Release* 117 (2) (2007) 227–237.
- [39] Z. Trajanoski, L. Schaupp, M. Ellmerer, G.A. Brunner, T.R. Pieber, A. Wutte, F. Skrabal, P. Wach, Interstitial fluid sampling using open flow microperfusion of subcutaneous adipose tissue, 18th Annual International Conference of the IEEE: Engineering in Medicine and Biology Society, Amsterdam, Netherlands, 1996.
- [40] S.S. Iyer, W.H. Barr, M.E. Dance, P.R. Coleman, H.T. Karnes, A 'biorelevant' system to investigate *in-vitro* drug release from a naltrexone implant, *Int. J. Pharm.* 340 (1–2) (2007) 104–118.
- [41] L.A. Pagliaro, A.M. Pagliaro, *Psychologists' psychotropic drug reference*, Brunner/Mazel, Philadelphia, 1998.
- [42] D.V. McAllister, P.M. Wang, S.P. Davis, J.-H. Park, P.J. Canatella, M.G. Allen, M.R. Prausnitz, Microfabricated needles for transdermal delivery of macromolecules and nanoparticles: fabrication methods and transport studies, *Proc. Natl. Acad. Sci. U. S. A.* 100 (2003) 13755–13760.
- [43] M. Davidian, D.M. Giltinan, *Nonlinear models for repeated measurement data*, CRC Press, Boca Raton, 1995.
- [44] C.R. Robbins, *Chemical and physical behavior of human hair*, Springer, 2002.